Journal of Materials Chemistry B

Accepted Manuscript

ROYAL SOCIETY OF CHEMISTRY

www.rsc.org/materialsB

Single step synthesis of carbon dots embedded chitosan nanoparticles for cell imaging and hydrophobic drug delivery

Angshuman Ray Chowdhuri[1], Satyajit Tripathy[2], Chanchal Haldar[1], Somenath Roy[2], Sumanta kumar Sahu[*1]

1 Department of Applied Chemistry, Indian School of Mines, Dhanbad 826004, Jharkhand, India

2 Immunology and Microbiology Laboratory, Department of Human Physiology with Community Health, Vidyasagar University, Midnapore-721102, India

* Corresponding author. E-mail: sahu.s.ac@ismdhanbad.ac.in, sumantchem@gmail.com; Fax: +91 326-2307772; Tel: +91 3262235936

Abstract:

The florescent carbon dots conjugated chitosan nanoparticles are developed for the cellular imaging and delivery of poorly water soluble drug *telmisartan* (TEL). In this work, the florescent chitosan nanoparticles are synthesized in a single step. The presence of surface functional groups and conjugations of the nanoparticles are investigated by FTIR spectroscopy. Dynamic Light Scattering and TEM analysis are performed to determine the size of the nanoparticles. To investigate the surface morphology FESEM analysis is also performed. The cytotoxicity of the nanoparticles is examined by MTT assay using normal lymphocytes and KG1A cancer cell lines. The intracellular cellular uptake is studied by fluorescence microscopy and flow cytometry analysis. The interactions between the nanoparticles and the drug are investigated by Gaussian 09 and visualized by GaussView 5 program package.

Keywords: O-carboxymethyl chitosan nanoparticles; Carbon dots; Drug delivery; *Telmisartan*; Computational study; Controlled release.

1. Introduction:

Fluorescent nanoparticles have drawn increasing attention owing to their extensively use in fields of biotechnology, electronics, sensors and catalysis due to their high quantum yield and fluorescence color [1-4]. In the past few years, different types of fluorescent nanoparticles such as up-conversion fluorescent nanoparticles, semiconductor quantum dots, polymer fluorescent nanoparticles and liposome fluorescent nanoparticles were widely studied in diverse applications [5-8].

Recently, carbon dots have attracted much attention as a fluorescent material due to their desirable properties such as high fluorescence, aqueous solubility, facile functionalization, low toxicity and good biocompatibility [9, 10]. These properties make carbon dots as a promising material for numerous exciting applications such as drug delivery, bioimaging, biosensing and optoelectronic devices [11]. Till now, many methods have been developed to synthesis of the carbon dots [12, 13]. After synthesis, the carbon dots may be directly used for applications without any modification or may be combined with nanoparticles for different applications. Recently carbon dots are directly used by Niu et al., where nitrogen-doped carbon quantum dots are synthesized as a fluorescent probes for selective biosensing and bioimaging [12]. Simultaneously, Chandra et al. have prepared multi-structure nanocarbons from carbon xerogel for bio-imaging [14]. We have also synthesized a significantly high fluorescent nitrogen and phosphorus doped carbon dots for the Fe^{3+} ions detection in cancer cells [15]. At the same time carbon dots are indirectly used by Sahu et al. for camptothecin delivery and multimodal imaging [16]. We have synthesized carbon dots conjugated silver nanoparticles to investigate the enhanced antibacterial activity [17]. Simultaneous synthesis and conjugation of carbon dots with nanoparticle have not been widely reported in the literature. Developing of simple methods for synthesizing nanoparticle conjugated carbon dots in a single step is still a great challenge.

Chitosan, a natural copolymer obtained by deacetylation of chitin, has attracted particular attention as a drug carrier. It demonstrates good biocompatibility, biodegradability and non-toxicity [18, 19]. Presently chitosan nanoparticles are widely used in drug delivery systems [20-23]. The smart drug delivery systems are needed to reduce the toxic side effects, improve drug loading efficiency and reduce the burst release of drug molecules [24]. When designing a drug

delivery system, it is important to take into account the conjugation of fluorescent molecules with nanoparticles (NPs). This conjugation is highly depends on chemical structure of fluorescent molecules and functional groups present on the NPs. Mohapatra et al. have chosen rhodamine isothiocyanate as a florescent probe in multifunctional mesoporous hollow silica nanocapsules for targeted co-delivery [25], while Zhang et al. have reported chitooligosaccharide based polymeric nanoparticles as drug carriers for co-delivery of all-trans-retinoic acid and paclitaxel with fluorescein isothiocyanate [26]. Recently we have also developed chitosan nanoparticles for targeted drug delivery systems [27]. To prove the targeted drug delivery systems, we had conjugated different fluorescent molecules with chitosan nanoparticles. However, there was a tedious multistep synthetic route for the reported fluorescent nanoparticles, which inspired us to investigate the synthesis of fluorescent nanoparticles in a facile way. Recently fluorescent carbon dots are synthesized from chitosan for bioimaging [28, 29]. In this context, we have developed a single step method to synthesize the fluorescent chitosan nanoparticles for hydrophobic drug delivery.

Telmisartan (TEL), belonging to an angiotensin II receptor antagonist, is used as an anti-hypertensive drug for the treatment of arterial hypertension. TEL is a hydrophobic drug with poor aqueous solubility. To increase its solubility, TEL is currently formulated with different types of nanoparticles. Zhang et al. have decorated mesoporous silica nanoparticles for oral delivery of the TEL, simultaneously Tran et al. have reported self-assembled gelatin–oleic acid nanoparticles for enhancing bioavailability of poorly water soluble drug *Telmisartan* [30, 31].

The aim of our study was to develop a facile process to synthesize a fluorescent nanoparticle having good biocompatibility and ability to carry the hydrophobic drugs. Here methyl methacrylate (MMA) grafted chitosan copolymeric nanoparticles are synthesized, where MMA acts as a hydrophobic moiety and chitosan as a hydrophilic moiety. We have used PMMA due to easy nanoparticles formation with hydrophilic OCMC by graft copolymerization in aqueous solution. The core of the nanoparticle is hydrophobic due to PMMA and the hydrophilic shell is formed by OCMC. The synthesized particles are spherical in shape, well dispersed and having a hydrophobic drug loading capability. At the same time carbon dots are produced from chitosan and immobilized on the surface of the nanoparticle. The physicochemical properties of

synthesized nanoparticles were characterized by Fourier transform infrared (FTIR) and fluorescence spectroscopy. The surface morphology of nanoparticles was characterized by field emission scanning electron microscopy (FESEM). As a hydrophobic anti-hypertensive drug, *telmisartan* (TEL) was loaded into the nanoparticles through electrostatic interaction. The loading capacity as well as the loading efficiency was investigated, and *in vitro* release profiles were studied. The density functional theory (DFT) calculation using Gaussian 09 and GaussView 5.0 program supported the electrostatic interaction phenomena between O-carboxymethyl chitosan nanoparticle and TEL.

2. Materials and Method:

2.1. Materials Used

Chitosan powder (CS) (Mw = 100,000–300,000, deacetylation degree ≥ 90% as determined by free amine groups), 3-(4, 5-dimethylthiazol-2-yl)-2, 5-diphenyltetrazolium bromide (MTT), dialysis bag (MWCO 14000 Da) and model drug *Telmisartan* were purchased from Sigma Aldrich. Methyl methacrylate (MMA) was acquired from alfa aesar. Ammonium persulfate (APS), sodium hydroxide, monochloroacetic acid, isopropanol and methanol were obtained from Merck India, water was millipore water. All Chemicals were used without further purification. Minimum essential medium (MEM) and fetal bovine serum were procured from Himedia, India and Hyclone, USA respectively.

2.2. Preparation of O-carboxymethyl chitosan (OCMC)

Here O-carboxymethyl chitosan was synthesized by a formerly reported method with a slight modification [32]. Briefly 0.5 g of chitosan is softened in 20 mL 50% sodium hydroxide solution at 0 °C for 24 h. Then the swelled chitosan was washed with isopropanol and dissolved in 20 mL of isopropanol. After that 1.5 g of monochloroacetic acid was dissolved in 3 mL of isopropanol, and added drop wise into the above solution for 30 min and reacted for 15 h at the 35 °C. Then the reaction was stopped by adding 25 mL of 70 % ethyl alcohol. The white product was filtered and washed with ethyl alcohol and vacuum dried at 40 °C. The resultant product was sodium salt of O-carboxymethyl chitosan.

2.3. Preparation of O-carboxymethyl chitosan nanoparticles (OCMC-MMA NPs)

O-carboxymethyl chitosan nanoparticles (OCMC-MMA NPs) were prepared according to the previous report [33], via grafting copolymerization. In brief, 1.0 g of as synthesized OCMC was dissolved in 100 mL water, into which 0.5 g of MMA monomer was added under argon atmosphere. After the complete mixing, 5% of ammonium persulfate (APS) solution (1 mL) was added very slowly under stirring condition. The reaction was carried out in inert atmosphere at 70 °C for 24 h. The obtained OCMC-MMA nanoparticles were dialyzed (MWCO 14000 Da) against water and lyophilized.

2.4. Preparation of florescent carbon dots embedded OCMC-MMA NPs (OCMC-MMA NPs/CDs)

To prepare the florescent carbon dots (CDs) attached OCMC-MMA NPs, first OCMC-MMA NPs were prepared by above mentioned procedure and then the temperature of the OCMC-MMA nanoparticles solution system was enhanced to 150 °C. The temperature was maintained at 150 °C, for the carbonization of free OCMC. After 10 h stirring, the solution was cooled down to room temperature and brown colored solution of carbon dots was observed. The brown colored solution was centrifuged in 18000 rpm for 15 min and obtained final solution was dialyzed against water with a dialysis bag (MWCO 14000 Da) to obtain highly fluorescence carbon dots attached nanoparticle solution. To optimize the reaction condition for synthesis of OCMC-MMA NPs/CDs, synthesized OCMC-MMA NPs solution was treated under three different temperatures **(**105 °C, 120 °C, and 135 °C).

2.5. Telmisartan drug loading

TEL loaded OCMC-MMA NPs were prepared by dialysis method using probe-type ultrasonicator [34]. 10 mg of OCMC-MMA NPs were gradually added to TEL solution (10 mg/10 mL) in ethanol under magnetic stirring. The mixture was dispersed for 10 min in ice bath by a probe-type ultrasonicator, followed by dialysis against distilled water for 12 h using a

dialysis bag (MWCO 14000 Da). Dialyzed products were centrifuged at 18000 rpm for 10 min to remove the free TEL and then freeze-dried to obtain the TEL-loaded OCMC-MMA NPs. The actual amount of loaded *telmisartan* was calculated spectrophotometrically at 295 nm with a UV-1700 spectrophotometer (Shimadzu). The drug loading content and entrapment efficiency were calculated according to the following equations.

$$\text{Drug loading contents (\%)} = \frac{\text{Weight of drug in nanoparticles}}{\text{Weight of nanoparticles taken}} \times 100$$

$$\text{Drug Entrapment Efficiency (\%)} = \frac{\text{Weight of drug in nanoparticles}}{\text{Weight of total drug injected}} \times 100$$

Percentage of drug entrapment efficiency was 82.9 % and drug loading content was 28.2 %.

2.6. *In vitro* Release of TEL from nanoparticles solution

The cumulative release behavior of poorly water soluble drug, *telmisartan* from the synthesized nanoparticles were investigated in the dissolution medium containing phosphate-buffered saline (PBS buffer 7.4) at 37 °C. The freeze-dried *telmisartan* loaded nanoparticles were weighed and resuspended in a tube containing 20 mL of PBS buffer solutions. TEL loaded NPs (10 mL) were placed in a dialysis bag (MWCO 14000 Da), which were immersed in 250 mL PBS (pH 7.4) and kept at 37 °C and 1200 rpm. At predetermined time intervals, aliquots of 4 mL were taken out and replaced with an equal volume (4 mL) of fresh PBS release medium. The amount of released TEL was determined by UV-Vis spectroscopy at 295 nm.

2.7. Computational details

The density functional theory (DFT) calculation using Gaussian 09 and GaussView 5.0 program investigated the electrostatic interaction phenomena between nanoparticle and the drug,

TEL. All the calculations were executed by Gaussian 09 suite of codes using a personal computer. For visualization GaussView 5.0 molecular visualization program was used. Gas phase molecular structure of the drug *telmisartan* and polymer chitosan in the ground state was optimized by DFT in its restricted forms without any symmetry constrain. To produce accurate ground state geometry of drug *telmisartan*, three chain long OCMC-MMA and TEL conjugated OCMC-MMA complexes were minimized by using B3LYP/6-31G (d) basis set. Frequency calculation at the same level of theory was performed to ensure that the equilibrium system represents minimized geometry. To reduce the excess computational load three chain long carboxymethyl chitosan-MMA was considered as equivalent to methyl methacrylate grafted chitosan copolymer.

2.8. *In vitro* Cytotoxicity Study

In vitro cytotoxic effect of the carbon dots conjugated OCMC-MMA NPs was studied on peripheral blood lymphocytes and acute myeloid leukemia cell, KG-1A using 3-(4, 5-dimethyl-2-thiazolyl)-2, 5-diphenyltetrazolium bromide (MTT) assay. The cells were seeded ($2x10^4$/mL) in 96 well plates and incubated at 37 °C under 5% CO_2 for 24 h. After satisfactory growth of the cells, growth medium was replaced with the respective test solutions and incubated. Finally, nanoparticles solution was replaced with MTT (150 µg/mL). Cells were incubated for 2 h at 37 °C to initiate formation of the formazan. After completion of the reaction, medium was replaced with 300 µL of DMSO (Sigma, USA). This conjugate was agitated moderately to dissolve formazan crystals. Finally, the dissolved formazan in DMSO was transferred into fresh 96 well plates and read on microplate reader (Thermo, USA) at 570 nm [35].

2.9. Bio-imaging of cellular uptake

To examine the bare OCMC-MMA NPs/CDs incorporation into the normal and cancer cells, nanoparticles were exposed into the cell culture media [36]. Each culture was incubated in an incubator at 37 °C for 4 hrs. The cells were washed twice by phosphate buffered saline to remove any unutilized nanoparticles. The fluorescence intensity of each sample was analyzed under fluorescent microscope for detection of internalization of nanoparticles in to the cells.

2.10. FACS study for cellular uptake

To be confirmed about the intracellular uptake the OCMC-MMA NPs/CDs exposed normal and cancer cells were analyzed by flow cytometry using florescent carbon dots conjugated OCMC-MMA NPs. For each sample, 100,000 cells were analyzed with FACSCalibur (BD, USA) using the CellQuestPro software.

2.11. Data analysis

The statistical analysis was executed by using a statistical package, Origin 6.1, Northampton, MA 01060, USA) with student's *t* tests, $p < 0.05$ as a limit of significance.

2.12. Characterization

Attachments of surface functional groups of CS, OCMC, lyophilized OCMC-MMA NPs, TEL and TEL conjugated OCMC-MMA NPs were investigated by Fourier transform infrared spectroscopy (FTIR) spectroscopy (Thermo Nicolet Nexux FTIR model 870) at room temperature. To investigate the surface morphology, Field Emission Scanning Electron Microscopy (FESEM) analysis was performed by using Supra 55 with Air Lock chamber for scientific research. The morphological examination of OCMC-MMA NPs and OCMC-MMA NPs/CDs was accompanied by Transmission Electron Microscopy (TEM) (H-600A, Hitachi, Japan). The samples were dispersed with water-ethanol and placed on carbon coated copper grids, which were completely air-dried and negative stained by using 1% (w/v) phosphotungstic acid prior to the analysis. The characteristics emission spectra of florescent chitosan nanoparticles at different excitations were recorded by Perkin Elmer LS 55 Fluorescence Spectrometer. The NPs were dispersed in 0.2 M phosphate buffered solution (PBS, pH 7.4) and ultrasonicated to determine the average hydrodynamic particle size by dynamic light scattering using using Zetasizer Nano ZS90 (Malvern, UK) at 25 °C. The fluorescence intensity of each sample was analyzed by fluorescent microscope (HITACHI 7400) for the detection of fluorescence intensity in cells (excitation and emission wavelengths were 495 nm and 529 nm respectively). To determine the conjugation of PMMA towards OCMC is confirmed by 1HNMR using BRUKER ADVANCE II 400 NMR spectrophotometer.

3. Results and Discussion

Recent advances in fluorescence imaging have simplified the investigation of biosynthetic and endocytic pathways in great detail for a complete understanding of intracellular drug delivery both *in vivo* and in vitro. Now carbon dots are studied for real-time dynamics of cellular components and pharmacological agents to traffic within the single cell [37]. Here, we have designed the nanoparticles for intracellular hydrophobic drug delivery from the perspective of fluorescence imaging by conjugating carbon dots as illustrated in fig.1. To prepare the nanoparticles, first OCMC was successfully prepared. Then amphiphilic OCMC nanoparticles were synthesized through the graft copolymerizion and self-assembly between hydrophilic OCMC and hydrophobic MMA. After that the carbon dots were embedded onto the nanoparticles along with optimization at different temperature. The attachment of carbon dots to the surface of OCMC nanoparticles is basically an electrostatic interaction.

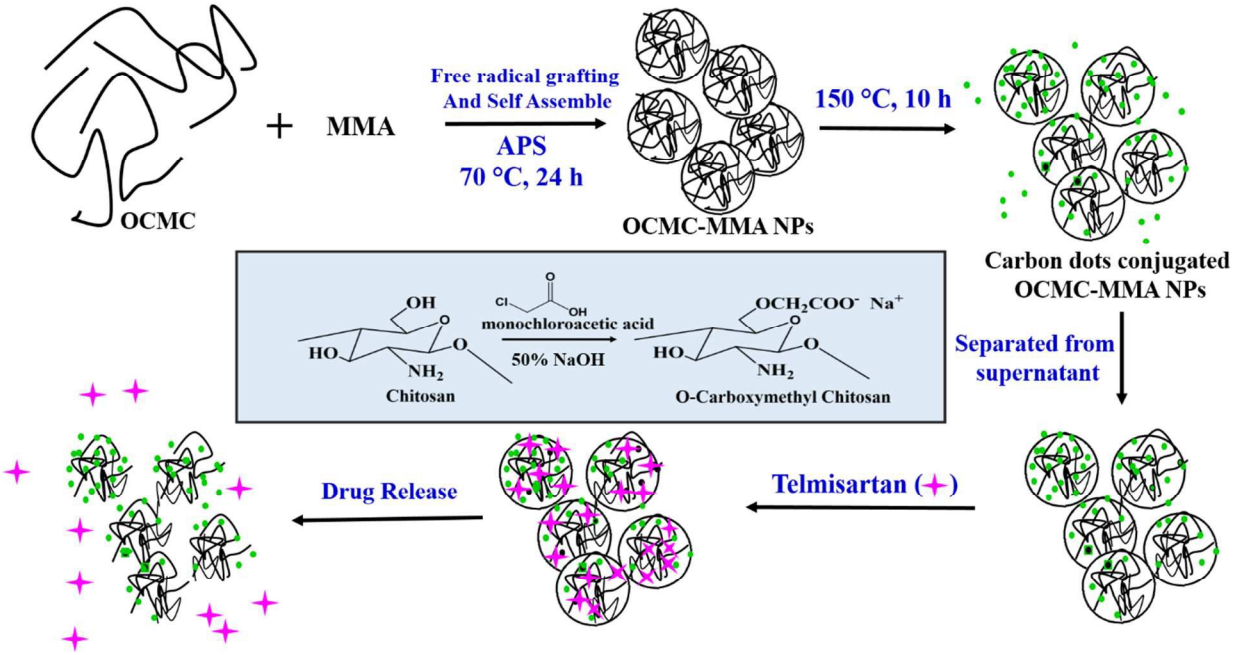

Fig. 1. Schematic representation of the synthesis of present drug delivery vehicles.

3.1. FTIR Analysis

The characteristics surface functional groups of the nanoparticles and drug conjugation were investigated by FTIR study. The FTIR spectra of pure CS, OCMC, OCMC-MMA NPs and TEL conjugated OCMC-MMA NPs are presented in fig. 2. The basic characteristics peaks of CS at 3455cm^{-1} (O–H stretch), 2900cm^{-1} (C–H stretch), 1648 cm^{-1} for amide I (N–H bend), 1154cm^{-1} (bridge –O– stretch), and 1094cm^{-1} (C–O stretch) are shown in fig. 2 (a) [38]. The FTIR spectrum of OCMC (fig. 2 (b)) shows a broad band at 3420 cm^{-1} due to the stretching vibrations of amine and hydroxyl groups, peaks at 1740 cm^{-1} and 1629 cm^{-1} correspond to the stretching vibrations of carbonyl and protonated amino groups and a sharp peak at 1320 cm^{-1} is due to C-O stretching frequency [39]. The result indicates that the carboxymethyl groups have been successfully conjugated onto the chitosan backbone. Fig. 2 (c) shows the FTIR spectrum of OCMC-MMA nanoparticles. Characteristic peaks at 1149 cm^{-1} and 1069 cm^{-1} were due to the absorption bands of saccharine structures. A strong peak at 1733 cm^{-1} due to the ester bond of MMA confirmed the successful grafting polymerization between the OCMC chain and the MMA [33]. Fig 2 (e) and fig 2 (d) show the stretching frequencies of TEL and the TEL conjugated OCMC-MMA nanoparticles.

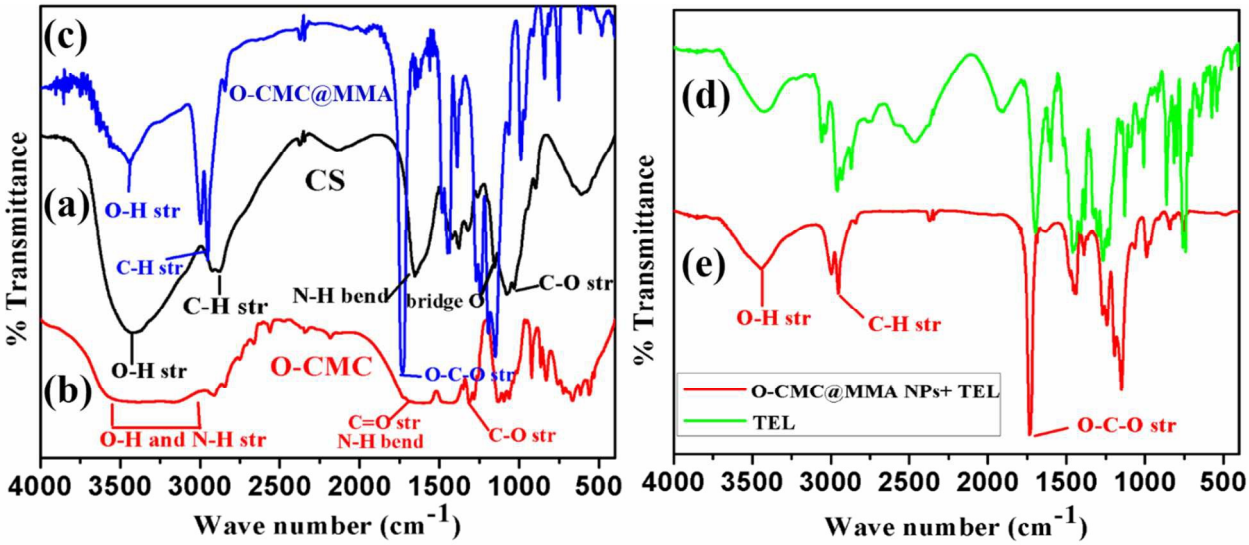

Fig. 2. FTIR spectra of CS (a) OCMC (b) OCMC-MMA NPs (c) TEL (d) TEL conjugated OCMC-MMA nanoparticles (e).

3.2. Surface Morphology Study

The actual size and shape of these self-assembled nanoparticles were determined by the FESEM and TEM analysis. The typical FESEM images of OCMC-MMA NPs prepared at temperature 70 °C are presented in fig. 3 (a). It is confirmed from the FESEM image that particles are uniform in shape and the size is about 45±10 nm. When the temperature were raised from 70 °C to 105 °C, some of carbon dots were formed *in situ* from the unreacted carboxymethyl chitosan and attached to the surface of the OCMC-MMA nanoparticles as shown in fig. 3(b) . Fig 3(c) and fig. 3 (d) show the conjugation of the carbon dots to the nanoparticles at 135 °C and 150 °C respectively. With raising the temperature, the formation of carbon dots is increasing and also confirmed by the PL spectroscopic study. The surface morphology of the nanoparticles is again examined by TEM micrographs and it is correlated with the FESEM image. The polymeric nanoparticles synthesized at 70 °C were well dispersed, spherical in shape with an average particle size of 35±10 nm, shown in fig. 3 (e). This size of the nanoparticles is actually between the favored ranges of the effective drug-delivery [40]. The attachments of *in situ* formed carbon dots to the OCMC-MMA nanoparticles at 105 °C, 135 °C and 150 °C temperature are perfectly showed in fig. 3 (f), fig. S1 (a) and (b) respectively (ESI). The average hydrodynamic size of the nanoparticles was determined by DLS measurement is shown in fig. S2 and fig. S3 (ESI). The obtained result revealed that the hydrodynamic size of the nanoparticles is 100-200 nm. The DLS study was carried out in the swollen state of the nanoparticles in water and TEM study was in the collapse form of the nanoparticles. So, the size distribution obtained from DLS study is 3 to 4 times higher than TEM images.

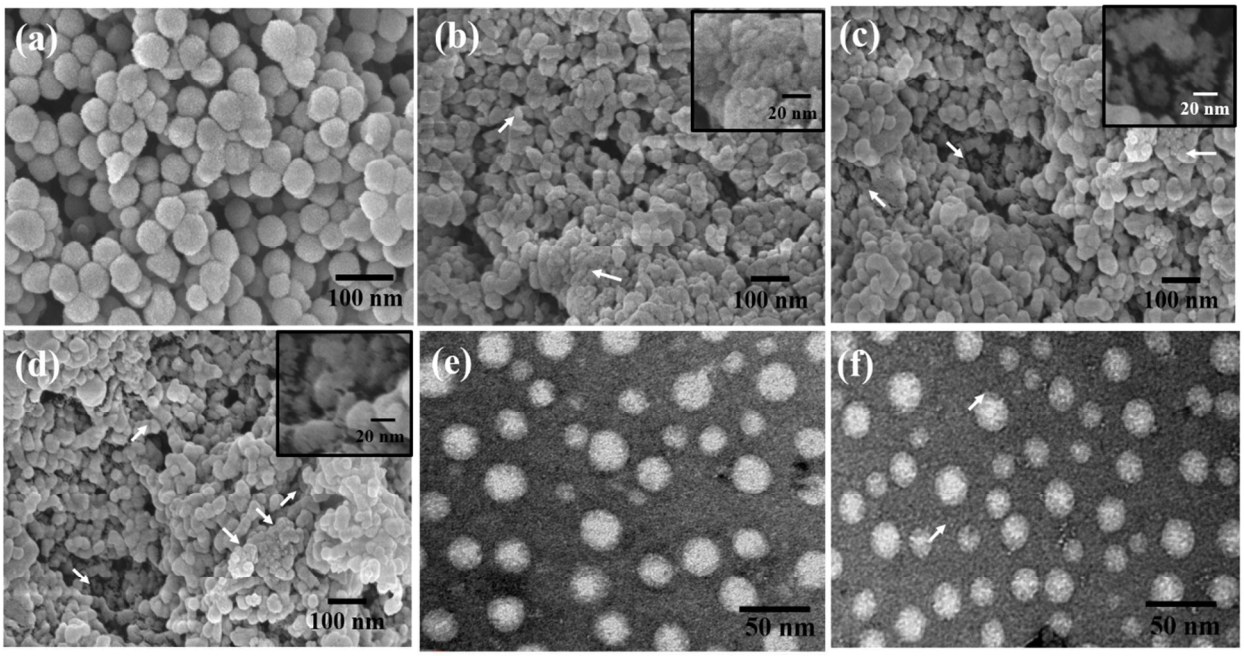

Fig. 3. FESEM images of carbon dot embedded OCMC-MMA nanoparticles synthesized at temperature 70 °C (a), 105 °C (b), 135 °C (c), 150 °C (d) and TEM images of carbon dot embedded OCMC-MMA nanoparticle synthesized at 70 °C (e) and 105 °C (f).

3.3. Florescence Study

To determine the characteristics fluorescent behavior of the aqueous solution of carbon dots conjugated OCMC-MMA NPs, the PL study is carried out with variable excitation wavelengths as shown in fig. 4(a). The result exposes that the CDs formed from carboxymethyl chitosan exhibits excitation independent as well as broad emission spectra. Recently, carbon dots are synthesized from chitosan showing the fluorescence emission spectra by varying the excitation wave length 340 nm to 410 nm [28]. Here from the emission spectra of the CDs, it is confirmed that CDs in aqueous solvent possess strong as well as broad PL emission centered at 430 nm, when CDs are exited at 340 nm. The optimization of florescence with four different temperature as 105 °C, 120 °C, 135 °C and 150 °C is shown in fig. 4(b). The high florescence intensity is observed at the temperature 150 °C and further enhancing temperature, there is no any obvious change in florescence intensity.

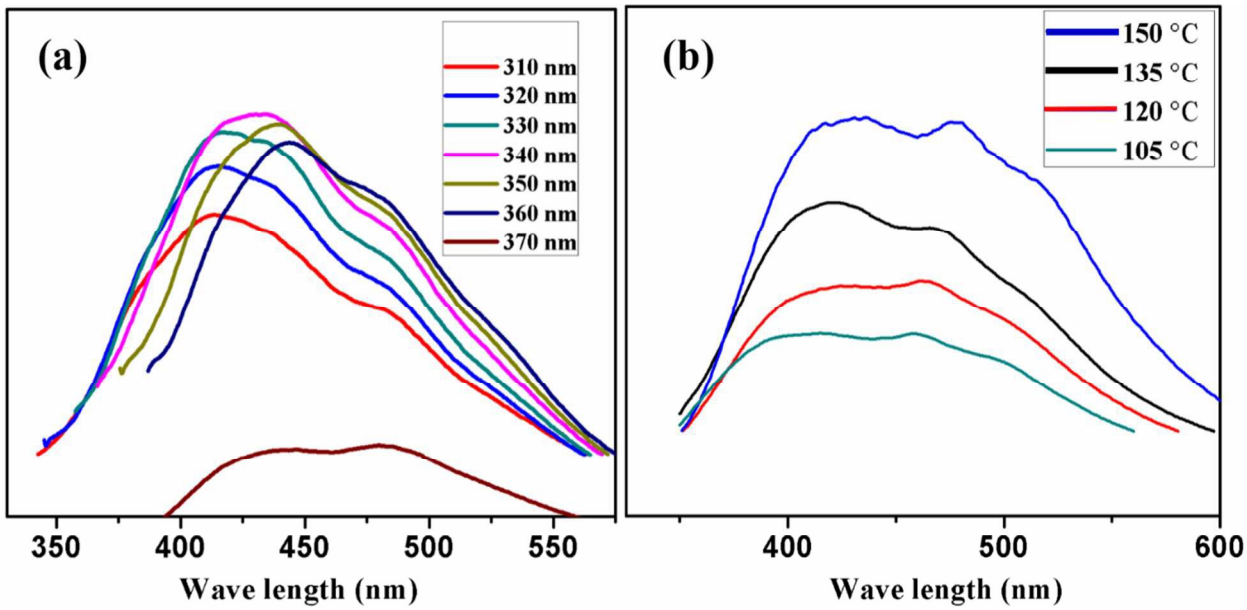

Fig. 4. Photoluminescence spectra of the synthesized OCMC-MMA@CDs at different excitations (a) and the optimization of OCMC-MMA@CDs at different temperature, excitation at 340 nm (b).

3.4.Geometry Optimization

Optimized electronic structure of drug *telmisartan*, three chain long OCMC-MMA and *telmisartan* conjugated OCMC-MMA (telmisartan@OCMC-MMA) complexes were calculated by hybrid DFT method B3LYP using 6-31G (d) basis set, shown in fig. 5 (a), fig. 6(a) and fig. 7 respectively. Drug *telmisartan* adopt a twisted half circular shape.

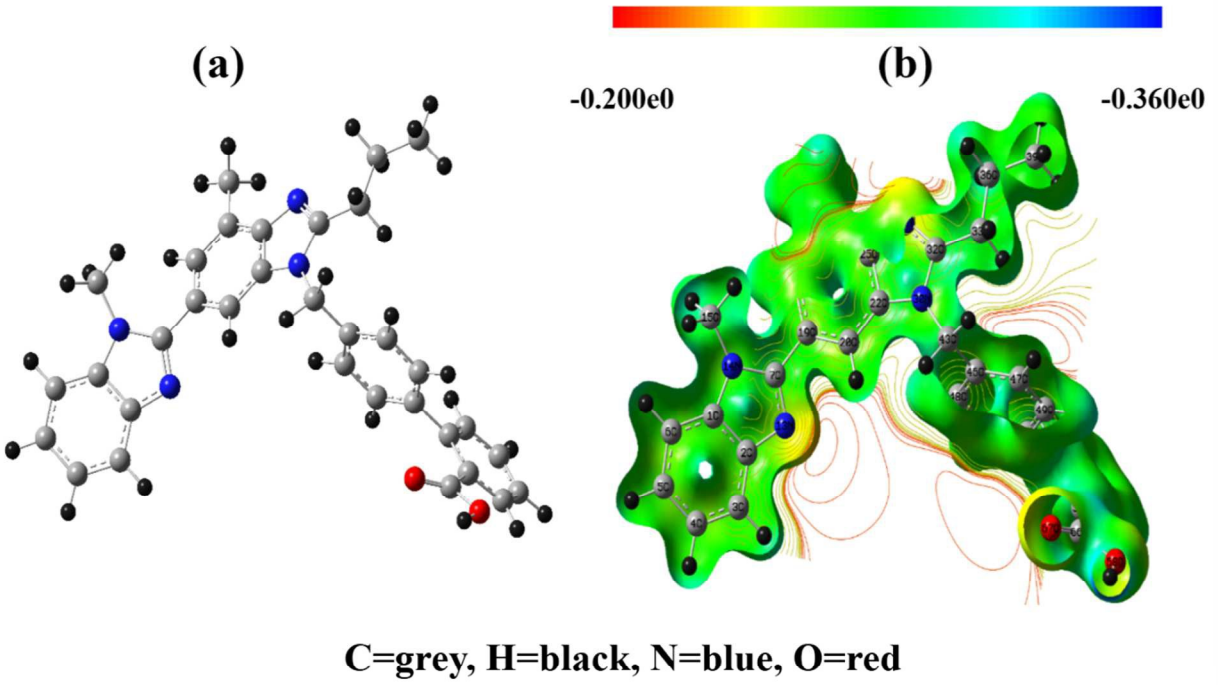

Fig. 5. (a) Optimized geometry of the drug *telmisartan* obtained at DFT/B3LYP/6-31G (d) level of calculation. (b) MEP of drug *telmisartan* obtained at the same level of theory with iso value 0.03.

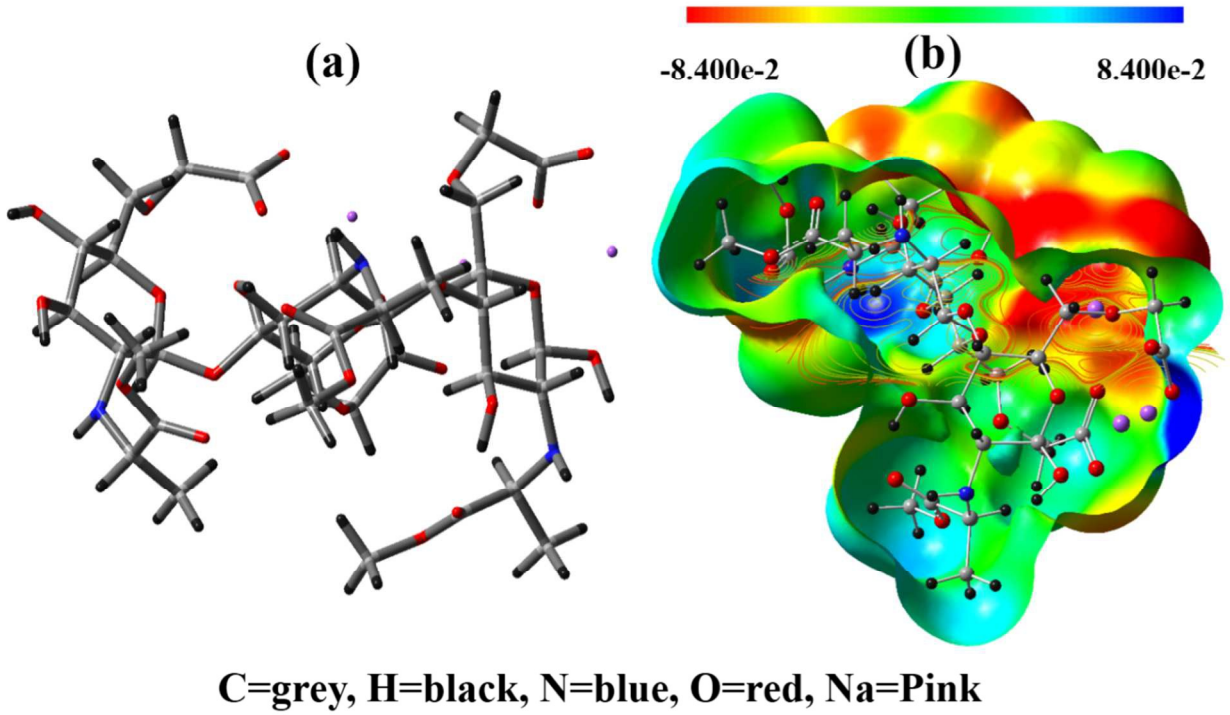

Fig. 6. (a) Optimized geometry of the OCMC-MMA (three chain long polymer) complex molecule obtained at DFT/B3LYP/6-31G (d) level of theory. (b) MEP map of chitosan with contours at iso value 0.03 calculated by the same level of theory.

In *telmisartan* dihedral angle between two benzimidazole moieties is 145.47° and dihedral angle between two benzene ring moieties is 56.65°. Benzimidazole strand and benzene ring strand were attached through -CH_2 group with a bond angle of 114.54°. Molecular electrostatic potential (MEP) of telmisartan exhibits an overall neutral charge distribution throughout the molecule as shown in fig. 5 (b). The yellowish region is indicating the presence of electronegative oxygen and nitrogen atoms in the molecule. Three chain long chitosan (shown in fig. 6 (a)) adopts distorted "H" shape, where each glucosamine ring is approximately right angle to the next glucosamine ring. Mobile Na^+ atoms are somewhat away from the main organic matrix making a specific region electropositive. MEP map (shown in fig. 6 (b)) of chitosan expresses its electrophilic and nucleophilic region. Intense blue surface is created due to the presence of Na^+ atoms while intense red surfaces are generated mainly due to the carboxylic acid groups.

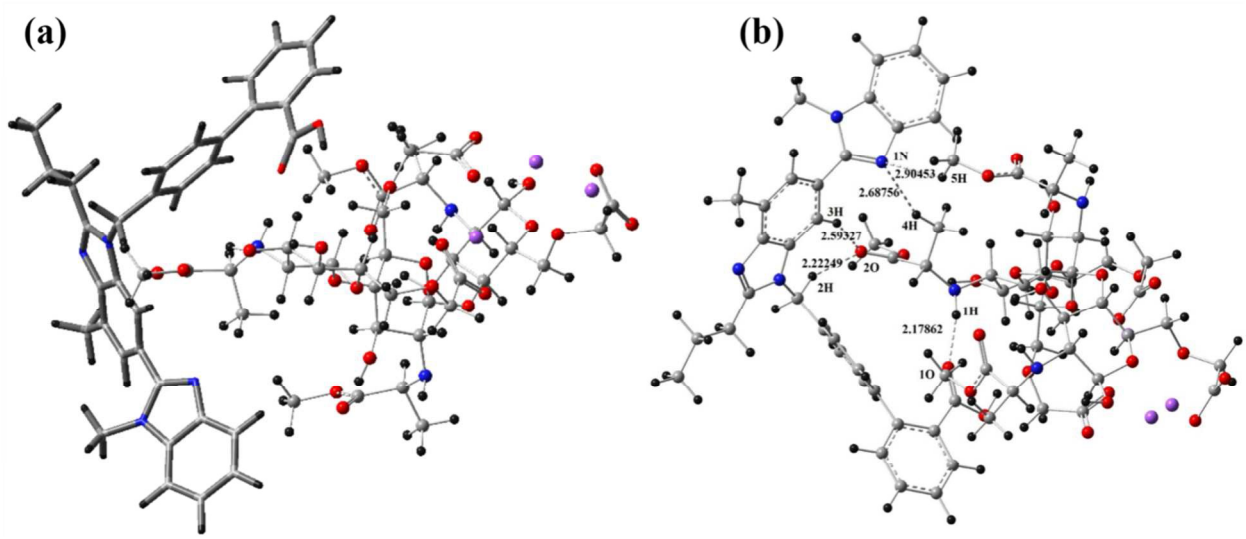

Fig. 7. (a) Optimized electronic geometry of telmisartan@OCMC-MMA complexe obtained at DFT/B3LYP/6-31G (d) level of theory. (b) Interacting sites in the telmisartan@OCMC-MMA complex.

3.5. Nature of Interaction

To examine the forces acting between the drug and polymer molecules, we have optimized the telmisartan@OCMC-MMA complex (shown in fig. 7 (a)). Absence of any usual covalent atomic distance (shown in fig. 7 (b)) between the atoms of two molecules eliminates the

existence of covalent bonding. We have estimated the electron affinity (EA) of *telmisartan* and chitosan molecules by ΔE method which is absolute energy differences between the anionic and neutral form of the optimized structures [41]. EA calculated by ΔE method was found to be -1.627374 Kcal/mol (-6.80893282 kJ/mol) and -0.508154 Kcal/mol (= -2.1261163 kJ/mol) for telmisartan and chitosan respectively. Low EA value suggests very less affinity towards accepting an electron. Presence of a number of aromatic ring makes the drug molecule *telmisartan* a little easy for accepting of an extra electron while polymeric compounds chitosan possess a large number of oxygen and nitrogen but show little greediness towards accepting an electron. Very small but negative value of EA makes both the molecules to act in a weak electrostatic interactions while eliminates the presence of an ionic type bonds.

Also we have calculated the amount of interaction energy/ stabilization energies for the formation of telmisartan@OCMC-MMA complex by applying the following equation.

$\Delta E_{interaction}$ (telmisartan@OCMC-MMA) = E (telmisartan@OCMC-MMA) - E (telmisartan) - E (OCMC-MMA)

Where $\Delta E_{interaction}$ (telmisartan@OCMC-MMA) = formation energy change of telmisartan@OCMC-MMA complex, E (telmisartan) = energy of telmisartan, and E (OCMC-MMA) = energy of chitosan.

The calculated interaction energy was found to be -10.92908 Kcal/mol. Zero point corrected interaction energy = -10.0126912 Kcal/mol (-41.8930999808 kJ/mol). This is much less than any reported covalent or ionic bond energy [42] suggesting no new covalent or ionic bond forms during the complexation. Two centered bond in the natural Lewis structure can also be identified from natural bond orbital (NBO) analysis [17]. Careful examination of NBO calculations does not indicate any effective bond between drugs and polymer molecules. Second order perturbation theory analysis shows a number of non-bonding interactions present within the telmisartan@OCMC-MMA complex. Some of the prominent interactions sites are listed in the table S1 (ESI). Among them LP (1) 1O→BD*(1) N-1H interaction energy 3.61 Kcal/mol and LP (1) 2O→BD*(1) C-2H interaction energy 3.22 Kcal/mol are the highest but still they are little less than the standard HO….H-OH_2 H-bonding energy (5.26 Kcal/mol) [42]. Other interactions

energy was found to be in the range [43, 44] of H-bond but considerably less than the standard H-bond energy.

Distance between interacting atoms and the interaction energy suggests the presence of at least two inter molecular H-bonding between drug and polymer molecules through 1O…1H-N and 2O…2H-C atoms. Other interacting positions may be considered as weak H-bonding or electrostatic interaction but definitely eliminate the possibilities of presence of any covalent bond. Although the second order perturbation energies (often called as the stabilization energies or interaction energies) of most of the non-bonding interactions are considerably very low. A large number of such non-bonding interactions, H-bonding or electrostatic interaction drags the *telmisartan* drugs molecules on the surface of OCMC-MMA polymer.

3.6. *In Vitro* Cytotoxicity Study

In vitro cytotoxicity studies showed that OCMC-MMA NPs/CDs were biocompatible on normal lymphocytes and cancer cell lines under ideal conditions of growth (shown in fig. S4). The results summarize impact of different dose dependent manner in comparison on OCMC-MMA NPs/CDs, to normal lymphocytes and KG-1A cancer cell in terms of percentage viability at various concentrations of test samples. More than 85% cells were found to be healthy after incubation with nanoparticles up to 500 $\mu g.mL^{-1}$.

3.7. Bio-imaging and intracellular Uptake of nanoparticles

Another significant property of OCMC-MMA NPs/CDs was realized in cellular imaging after 4 h of incubation as shown in fig. 8. The green fluorescing carbon dots conjugated OCMC-MMA nanoparticles are exposed (at 10 µg/mL concentrations) to normal lymphocytes and KG-1A under florescent microscope (at 100x). Nanoparticles were internalized inside the cells giving excitation dependent green florescence emission. This feature of CDs can be further used to fabricate molecular tags to view the site of infection when used along with molecular markers on the surface. It would be very interesting to understand the internalization mechanism of CDs into cells.

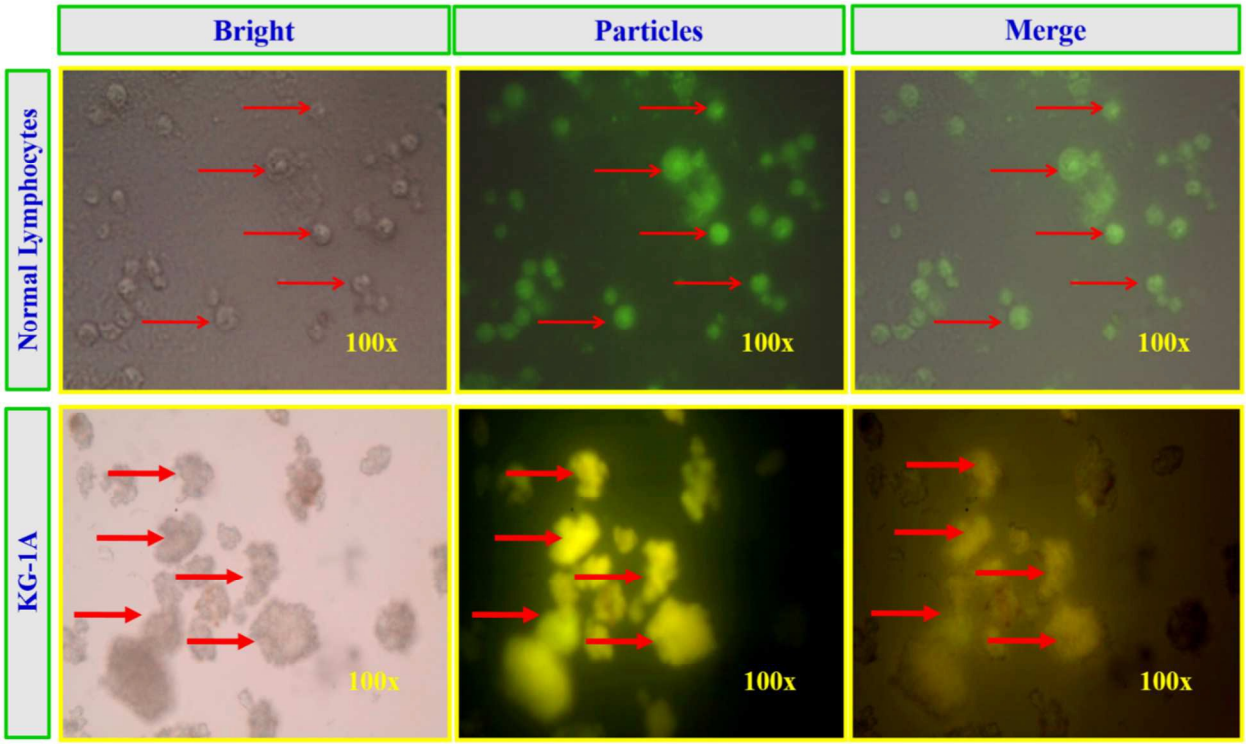

Fig. 8. Fluorescent Microscopic image (at 100× magnification) of particle uptake by normal lymphocytes and KG-1A cells.

Further the internalization of carbon dots conjugated OCMC-MMA NPs into cells flow cytometry (FACS) analysis was investigated. As shown by flow cytometry, OCMC-MMA NPs treated cells exhibited fluorescence intensity shifted from quadrant lower left to lower right in cases of normal lymphocytes (PBL) (Fig. 9a) and KG-1A (Fig. 9b). Observation of treated cultures revealed that OCMC-MMA NPs internalization is better in cancer cells (63.27%) then normal cells (56.7%) (Fig. 9c).

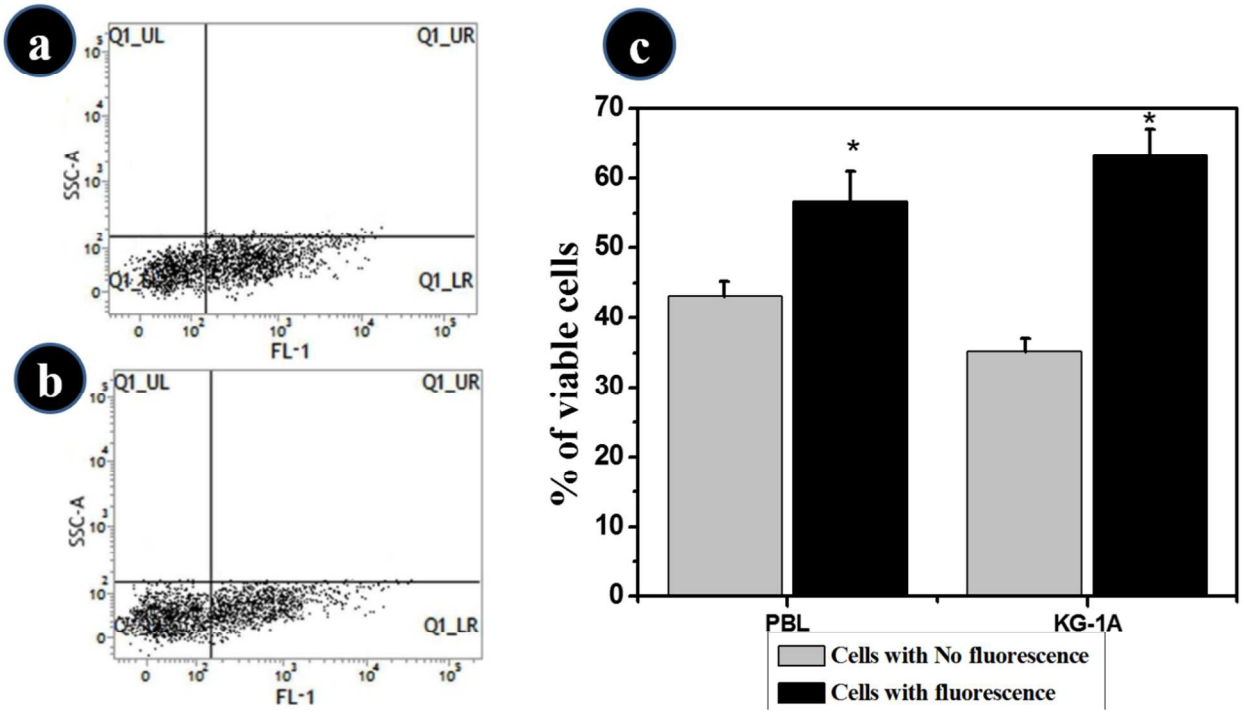

Fig. 9. FACS study for intracellular uptake of the OCMC-MMA NPs/CDs exposed normal and cancer cells (a) PBL, (b) KG-1A, (c) graphical presentation represents the comparison between the OCMC-MMA NPs/CDs uptake cells and OCMC-MMA NPs/CDs non uptake cells.

3.8. *In Vitro* Cumulative Drug Release

The loading content and entrapment efficiency of TEL in OCMC-MMA NPs are found to be 28.2 % and 82.9 % respectively. The loading of TEL into the OCMC-MMA NPs is due to the electrostatic interaction between the TEL molecules with the hydrophobic part of the OCMC-MMA NPs. The comparison of drug loading efficiency with relevant literature is mentioned in Table S2. The cumulative release performance is quite controlled with comparison to the other previous nanoparticles systems [45]. The release profile of the TEL from the nanoparticle was studied at physiological pH 7.4 at 37 °C. The drug release profile (shown in fig. S5) tells that about 26 % drug was released at first 10 h. About 41% and 61% drug was released after 30 h and 40 h respectively. After 92 h, 63% drug was released.

4. Conclusion

The biofriendly and green florescent carbon dots labeled hydrophobically modified OCMC-MMA NPs have been prepared by *in situ*. The amount of the carbon dots formation and florescent intensity could be easily controlled by regulating the temperature. The nanoparticles are very stable, less toxic and easily carry a high amount of poorly water soluble drug *telmisartan* with a controlled release capacity at pH 7.4. The electrostatic interaction between the nanoparticles and *telmisartan* is responsible for loading content of hydrophobic drug molecules. The interaction of the nanoparticles towards the cell and the intercellular uptake of the nanoparticles is investigated. To our knowledge, this is the first reported method to synthesize chitosan based florescent nanoparticles in a single step for hydrophobic drug delivery. In the future, the synthesized OCMC nanoparticles can be utilized promisingly in anticancer drug delivery, tumor cell detection and *in vivo* applications.

Electronic Supplementary Information (ESI)

TEM images of carbon dot conjugated OCMC-MMA nanoparticle synthesized at 135 ° C and 150 °C, DLS spectrum and size distribution of OCMC-MMA nanoparticles, Intermolecular interaction and second order perturbation energy (E (2), Kcal/mol) between donor and acceptor orbitals of Drug and copolymer molecules, Graphical representation of the cell viability towards normal lymphocytes and cancer cell after exposure with OCMC-MMA@CDs up to 500 μg/mL, In vitro *telmisartan* releases from OCMC-MMA@CDs at 7.4 pH solution. 1HNMR spectra of OCMC and OCMC-MMA NPs, The comparison of drug loading efficiency with relevant literature.

Acknowledgements

This work was financially supported by the DST, Government of India (SB/FT/CS-068/2013) and Indian School of Mines, Dhanbad.

References

1. C. I. Weng, H. T. Chang, C. H. Lin, Y. W. Shen, B. Unnikrishnan, Y. J. Li and C. C. Huang, *Biosensors and Bioelectronics*, 2015, 68, 1-6.
2. K. Zhang, G. Song, Y. Li, X. Wu, K. Li and B. Ye, *Sensors and Actuators B*, 2014, 191, 673-680.
3. J. Du, R. Zhao, Y. Xie and J. Li, *Applied Surface Science*, 2015, 346, 256-262.
4. X. Ren, L. Pang, Y. Zhang, X. Ren, H. Fan and S. Liu, *J. Mater. Chem. A*, 2015, 3, 10693-10697.
5. L. Zhou, X. Zheng, Z. Gu, W. Yin, X. Zhang, L. Ruan, Y. Yang, Z. Hu and Y. Zhao, *Biomaterials*, 2014, 35, 7666-7678.
6. H. S. Mansur, A.P. Mansur Alexandra, E. Curti and M. V. De Almeid, *Carbohydrate Polymers*, 2012, 90, 189-196.
7. S. K. Sahu, S. Maiti, T. K. Maiti, S. K. Ghosh and P. Pramanik, *Macromol. Biosci*., 2010, 11 (2), 285-295.
8. X. Zhang, S. Guo, R. Fan, M. Yu, F. Li, C. Zhu and Y. Gan, *Biomaterials*, 2012, 33, 7103-7114.
9. M. Liu, X. Zhang, B. Yang, Z. Li, F. Deng, Y. Yang, X. Zhang and Y. Wei, *Carbohydrate Polymers*, 2015, 121, 49-55.
10. C. Liu, P. Zhang, X. Zhai, F. Tian, W. Li, J. Yang, Y. Liu, H. Wang, W. Wang and W. Liu, *Biomaterials*, 2012, 33, 3604-3613.
11. K Hola. , Y. Zhang, Y. Wang, E. P. Giannelis, R. Zboril and A. L. Rogach, *Nano Today*. 2014, 9, 590-603.
12. W. J. Niu, Y. Li, R. H. Zhu, D. Shan, Y. R. Fan and X. J. Zhang, *Sensors and Actuators B*, 2015, 218, 229-236.
13. C. López, M. Zougagh, M. Algarra, C. E. Rodríguez, B. B. Campos, J.C.G. Esteves da Silva, J. J. Jiménez and A. Ríos, *Talanta*, 2015, 132, 845-850.
14. S. Chandra, S. Mitra, D. Laha, S. Bag, P. Das, A. Goswami and P. Pramanik, *Chem. Comm.*, 2011, 47, 8587-8589.
15. S. Chandra, D. Laha, A. Pramanik, A. Ray Chowdhuri, P. Karmakar & S. K. Sahu, *Luminescence*, 2015, DOI: 10.1002/bio.2927.

16. S. Sahu, N. Sinha, S. K. Bhuti, M. Majhic & S. Mohapatra, *J. Mater. Chem. B*, 2014, 2, 3799-3088.
17. Ray Chowdhuri, S. Tripathy, C. Haldar, S. Chandra, B. Das, S. Roy and S. K. Sahu, *RSC Adv.*, 2015, 5, 21515-21524.
18. M. Rajan and V. Raj, *Carbohydrate Polymers*, 2013, 98, 951-958.
19. J. L. Arias, L. H. Reddy and P. Couvreur, *J. Mater. Chem.*, 2012, 22, 7622-7632.
20. M. C. Chen, F. L. Mi, Z. X. Liao, C. W. Hsiao, K. Sonaje, M. F. Chung, L. W. Hsu and H. W. Sung, *Advanced Drug Delivery Reviews*, 2013, 65, 865-879.
21. Z. Liu, Y. Jiao, Y. Wang, C. Zhou and Z. Zhang, *Advanced Drug Delivery Reviews*, 2008, 60, 1650-1662.
22. S. K. Sahu, S. Maiti, T. K. Maiti, S. K. Ghosh & P. Pramanik, *Journal of Drug Targeting*, 2011, 19(2), 104-113.
23. M. E. Mathew, J. C. Mohan, K. Manzoor, S.V. Nair, H. Tamura and R. Jayakumar, *Carbohydrate Polymers*, 2010, 80, 442-448.
24. A. K. Patri, L. J. F. Kukowska and J. J. R. Baker, *Advanced Drug Delivery Reviews*, 2005, 57, 2203-2214.
25. S. Mohapatra, S. R. Rout, R. Narayan & T. K. Maiti, *Dalton Trans.*, 201443, 15841-15850.
26. J. Zhang, J. Han, X. Zhang, J. Jiang, M. Xu, D. Zhang and J. Han, *Carbohydrate Polymers*, 2015, 129, 25-34.
27. S. K. Sahu, S Maiti., A. Pramanik, S. K. Ghosh and P. Pramanik, *Carbohydrate Polymers*, 2012, 87, 2593-2604.
28. S. Chandra, S. H. Pathan, S. Mitra, B. H. Modha, A. Goswami and P. Pramanik, *RSC Adv.*, 2012, 2, 3602-3606.
29. D. Chowdhury, N. Gogoia and G. Majumdar, *RSC Adv.*, 2012, 2, 12156-12159.
30. Y. Zhang, J. Wang, X. Bai, T. Jiang, Q. Zhang and S. Wang, *Mol. Pharmaceutics*, 2012, 9, 505-513.
31. H. L. Tran Phuong, T. D. Tran Thao and B. J. Lee, *International Journal of Pharmaceutics*, 2013, 455, 235-240.
32. W. Yinsong, L. Lingrong, W. Jian and Q. Zhang, *Carbohydrate Polymers*, 2007, 69, 597-606.

33. L. Shi, C. Tang and C. Yin, *Biomaterials*, 2012, 33, 7594-7604.
34. X. Wang, Y. Chen, F. Z. Dahmani, L. Yin, J. Zhou and J. Yao, *Biomaterials*, 2014, 35, 7654-7665.
35. A. Ray Chowdhuri, S. Tripathy, S. Chandra, S. Roy & S. K. Sahu, *RSC Adv.*, 2015, 5, 49420-49428.
36. S. Tripathy, S. Chattopadhyay, S. K. Dash, A. Ray Chowdhuri, S. Das, S. K. Sahu, S. Majumdar and S. Roy, *International Journal of Biological Macromolecules*, 2015, 74, 585-600.
37. P. G. Luo, S. Sahu, S. T. Yang, S. K. Sonkar, J. Wang, H. Wang, G. E. LeCroy, L. Cao and Y. P. Sun, *J. Mater. Chem. B*, 2013, 1**,** 2116-2127.
38. Y. Li, S. Zhang, X. Meng, X. Chen and G. Ren, *Carbohydrate Polymers*, 2011, 83, 130-136.
39. S. Maya, S. Indulekha, V. Sukhithasri, K.T. Smitha, S. V. Nair, R. Jayakumar and R. Biswas, *International Journal of Biological Macromolecules*, 2012, 5, 392-399.
40. Y. Wang, Q. Zhao, N. Han, L. Bai, J. Li, J. Liu, E. Che, L. Hu, Q. Zhang, T. Jiang and S. Wang, *Nanomedicine: Nanotechnology, Biology, and Medicine*, 2015, 11, 313-327.
41. C. Amovilli, N. H. March, F. Bogár and T. Gál, Phys Lett A, 2009, 373(35), 3158-3160.
42. Shriver and Atkins, Inorganic Chemistry, Fifth Edition, *Oxford University press*, 2013, page No, 60, 87 and 285.
43. J. W. Larson and T. B McMahon, *Inorganic Chemistry*, 1984, 23 (14), 2029-2033.
44. J. Emsley, *Chemical Society Reviews*, 1980, 9 (1), 91-124.
45. W. Xu, J. Riikonen and V. P. Lehto, *International Journal of Pharmaceutics*, 2013, 453, 181-197.